Influence of local structures on the energy transfer efficiencies of quantum-dot films

Lintao Peng
Center for Nanoscale Materials, Argonne National Laboratory, Lemont, Illinois 60439, USA

Xuedan Ma*
Center for Nanoscale Materials, Argonne National Laboratory, Lemont, Illinois 60439, USA
and Consortium for Advanced Science and Engineering, University of Chicago, Chicago, Illinois 60637, USA

Hua Zhu and Ou Chen
Department of Chemistry, Brown University, Providence, Rhode Island 02912, USA

Wei Wang
Consortium for Advanced Science and Engineering, University of Chicago, Chicago, Illinois 60637, USA

(Received 17 March 2020; accepted 9 June 2020; published 27 July 2020)

Energy transfer is an important photophysical process that plays a significant role in determining the performance of many optoelectronic and light-harvesting devices. Combining carrier dynamics measurements with Monte Carlo simulations, we study the influence of local microscopic structures on energy transfer efficiencies in quantum-dot films. We find that in thin films, the formation of local domains leads to reduced energy transfer efficiencies, even though macroscopically the energy transfer rate remains intact. Compared to packing density, the vertical interlayer energy transfer has a small impact on the overall energy transfer efficiencies in our structures. In thick three-dimensional films, energy transfer outpaces biexciton recombination, suggesting the possibility to harvest multiexcitons in quantum-dot films for device applications.

DOI: 10.1103/PhysRevB.102.035437

I. INTRODUCTION

Förster resonance energy transfer (FRET), despite the long history since its discovery [1], retains its major role in many photophysical phenomena and applications. The specific distance dependence of FRET rates has been utilized to noninvasively measure intermolecular distances at the sub-10 nm scale in biological systems, which has otherwise been deemed inconceivable [2]. Energy transfer also plays an important role in many optoelectronic and light-harvesting devices. A key factor that determines the efficiencies of these devices is the long-range transport of excitons to designated dissociation sites and energy transfer is an efficient process in passing energy from one location to another. Utilization of energy transfer in photovoltaics has enabled the design of solar concentrators [3,4] and photosensitizers [5,6] that efficiently boost the solar cell quantum efficiencies.

In principle, FRET rate is directly proportional to the spectral overlap between donor emission and acceptor absorption spectra. Compared to energy transfer in organic dyes and biological molecules which have relatively broad absorption and emission spectra due to the closely lying vibrational levels, FRET in colloidal quantum dots (QDs) possesses a unique aspect. The size-dependent optical properties of QDs have led to a variety of applications including solar cells, light-emitting diodes, and lasers. Because of QDs' discrete energy levels caused by the quantum confinement effect, energy transfer in QD assemblies has been found to be much less efficient compared to that in chromophores [7,8]. The potential absence of nearby QDs with appropriate resonance energy levels could prohibit FRET considerably. Previous studies also show evidence that energy transfer rates in two-dimensional (2D) QD monolayers could be much faster compared to that in their three-dimensionally (3D) packed counterparts [9,10]. These observations highlight the important role that local film geometry, including the packing density and thickness, plays in determining the energy transfer (ET) efficiencies of a QD film, while macroscopic parameters, such as the overall energy transfer rate of the film, may not be sufficient to reflect the essence. The correlation between local film geometry and energy transfer efficiency therefore merits a thorough interrogation. Moreover, multiexciton states, a manifestation of many-body excitonic interactions that are closely related to the nonradiative Auger recombination process, prevail in large sized QDs even under weak irradiation [11–15]. Despite the important implication of these multiexciton states for optoelectronic device performance [13,16], little is known about their correlation with energy transfer in thin films.

Given the importance of energy transfer in QD films for their applications in optoelectronic and light-harvesting devices, we address these open questions by investigating the carrier dynamics of 2D and 3D QD films. For clarity, in this study, thin films with 1–2 monolayers of QDs are referred to as 2D films, whereas those with more than 4 monolayers of QDs are referred to as 3D films. Combining these measurements with Monte Carlo simulations, we find that ET

*xuedan.ma@anl.gov

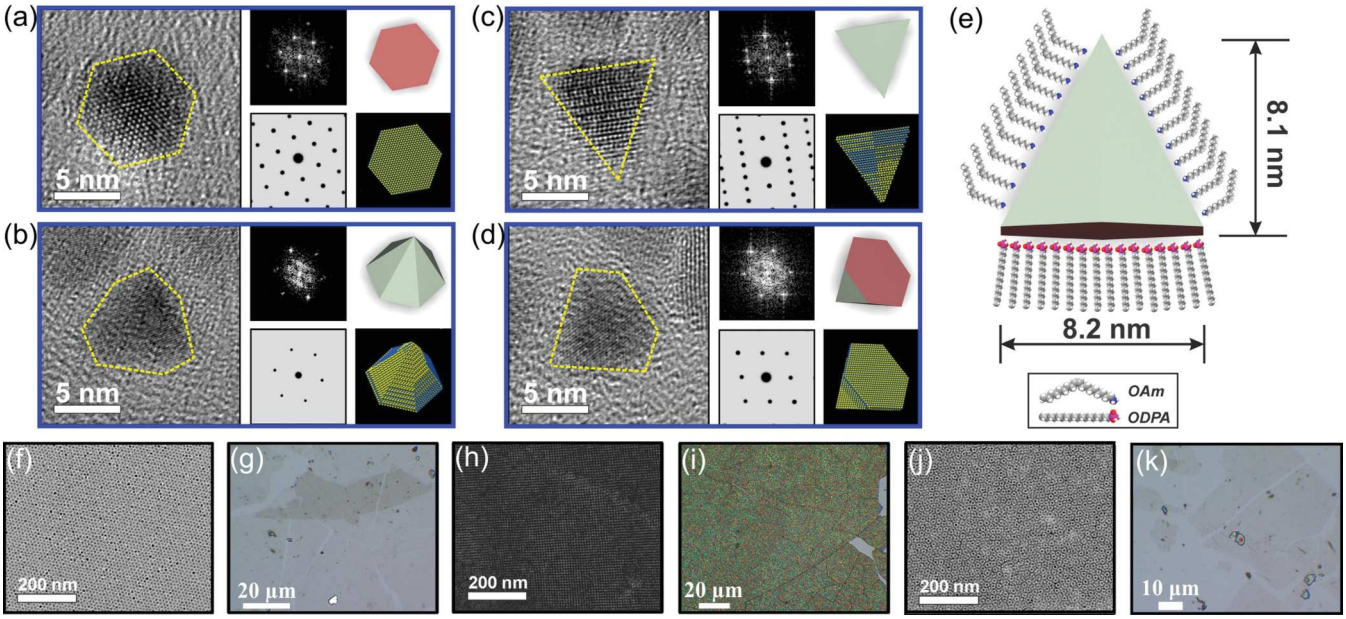

FIG. 1. (a)–(d) Four examples of hexagonal pyramid-shaped QDs with various orientations. For each of the examples, their high-resolution TEM images (left), the corresponding FFT patterns (middle top), the simulated electron diffraction patterns (middle bottom), and the corresponding structures derived from the patterns (right) are shown. (e) Sketch of a hexagonal pyramid-shaped QD with surface ligands. (f), (h), and (j) TEM images of 2D hexagonal packing (f), 3D fcc-like [viewed from [001] zone axis] (h), and 2D quasicrystalline (j) QD films. (g), (i), and (k) Corresponding optical micrographs of the 2D hexagonal packing (g), 3D fcc-like (i), and 2D quasicrystalline (k) QD films.

rates set an upper limit in the exciton propagation distance while perturbation to local geometry leads to less efficient ETs. Formation of in-plane domain boundaries results in smaller exciton propagation distances. In our structures, ET in the vertical interlayer direction has a small influence on the exciton propagation distance. The effective suppression of biexciton emission in 3D films suggests the potential for harvesting multiexciton states for optoelectronic applications. These findings have important implications for our understanding of energy transfer in QD films.

II. EXPERIMENT

QDs used in this study are hexagonal pyramid-shaped CdSe/CdS core-shell QDs synthesized following a previously reported method [17] (see the Supplemental Material S1 and S2 for details [18]). Figures 1(a)–1(d) show high-resolution TEM images, electron diffraction patterns, and the corresponding geometries of the QDs with different orientations. Their morphology is further illustrated in Fig. 1(e). We utilize this type of QDs due to their versatility to pack into 2D films of various crystalline arrangements [19,20], allowing our study of film structure-dependent ET processes, as we will discuss below. 2D QD films with hexagonal packing arrangements and 3D films with face-centered cubic (fcc)-like crystalline arrangements were prepared by slow-drying QD-cyclohexane solutions on ethylene glycol/water subphase [19,20] (see the Supplemental Material S1 for the detailed method [18]). For simplicity, in the following, we refer to these two types of films as 2D and 3D fcc films, respectively. 2D quasicrystalline superlattices with ten-fold symmetry containing 2 monolayers of QDs were prepared by slow-drying QD-cyclohexane solutions on ethylene glycol subphase. The QD films were then transferred onto silicon substrates for further characterizations. Figures 1(f) and 1(h) show TEM images of the 2D and 3D fcc QD films, respectively, and TEM images of the quasicrystalline 2D films are shown in Fig. 1(j). The uniform arrangement of the QD films can extend up to a few hundreds of micrometers on the substrates, as shown in the optical micrographs in Figs. 1(g), 1(i), and 1(k). Due to the 1–2 monolayer thickness of the 2D QD films in Figs. 1(g) and 1(k), their transparency allows the observation of the underneath silicon substrate.

To reduce the influence of electron-phonon interaction and thermal broadening on the photoluminescence (PL) spectra, we perform the optical measurements at 5 K. The prepared QD films were loaded into a cryostat on a home-built confocal laser microscope for spectroscopic measurements. A pulsed laser with a wavelength of 400 nm and a repetition rate of 2.5 MHz was used to excite the samples. Laser pulses were focused onto the samples using a microscope objective ($60\times$, NA $= 0.7$). Emission from the samples was collected by the same objective and sent to a charge coupled device installed on a 500 mm spectrograph for spectroscopic measurements, or to single-photon avalanche diodes for time-resolved measurements.

III. RESULTS AND DISCUSSION

A. Pump power-dependent photoluminescence spectroscopy

Figures 2(a) and 2(b) show the pump-dependent PL spectra of the 2D and 3D fcc films, respectively. Compared to the PL spectra of the 2D films [Fig. 2(a)], spectra of the 3D films are slightly redshifted [Fig. 2(b)], although both types of QD

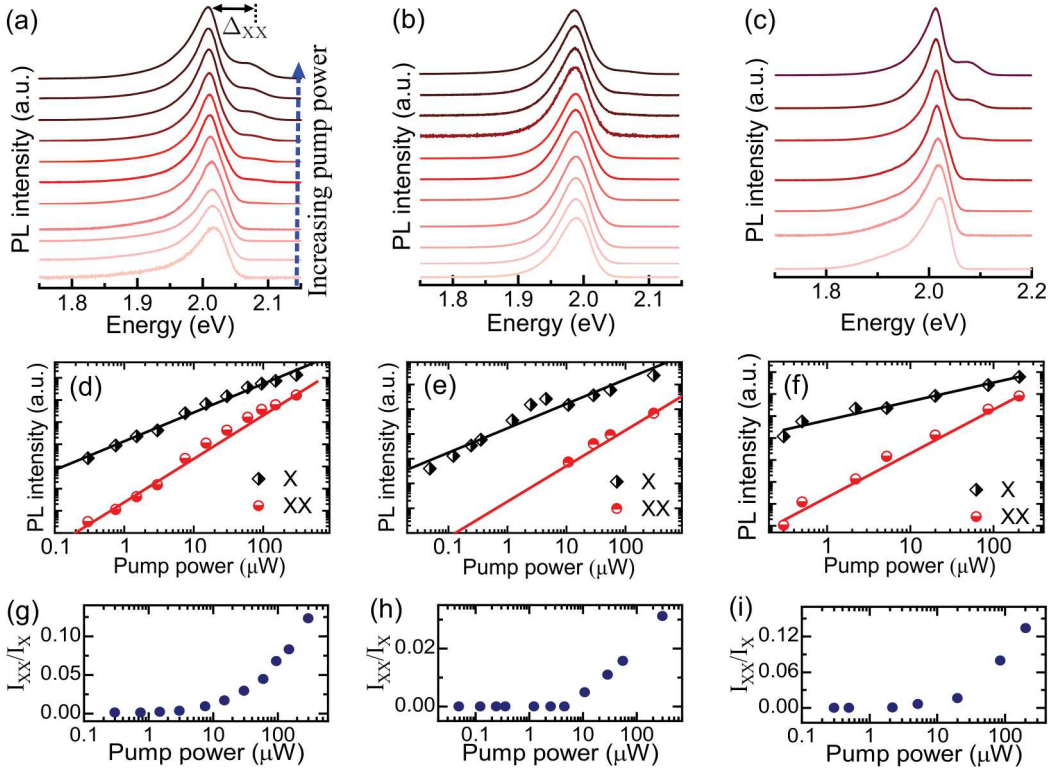

FIG. 2. (a)–(c) Pump-power dependent PL spectra of the 2D hexagonal packing (a), 3D fcc (b), and 2D quasicrystalline (c) films. For clarity, the spectra are normalized and offset. (d)–(f) Pump-power dependent integrated PL intensities of the single-exciton (X, black dots) and biexciton (XX, red dots) emission of the 2D hexagonal packing (d), 3D fcc (e), and 2D quasicrystalline (f) films. The lines are linear (black) and quadratic (red) fittings. (g)–(i) Integrated PL intensity ratios between the biexciton (I_{XX}) and single-exciton (I_X) emission of the 2D hexagonal packing (g), 3D fcc (h), and 2D quasicrystalline (i) films.

films show a long tail at the lower energy side. We note here that given the penetration depth of the excitation light in CdSe, we expect all the monolayers of the QDs in the 3D films to be excited. In QD assemblies, polydispersity in size exists even in "monodispersed" QD samples [21]. Photogenerated excitons in small QDs transfer their energies to proximity large QDs via dipole-dipole interactions [7]. Compared to noninteracting QDs, such an ET process can cause a redshift in the PL spectra, with the larger (smaller) QDs emitting toward the red (blue) side of the spectra [Fig. 3(a)]. The redshifted peak in the 3D films compared to that in the 2D films potentially indicates more efficient ET in the 3D films.

With an increasing pump power, a second peak with a separation energy of around 70 meV from the main peak starts to become more apparent on the high energy side in the 2D films [Fig. 2(a)]. The integrated PL intensities of the main peak at 2.01 eV and the newly emerged peak at 2.08 eV are plotted in Fig. 2(d), with the former showing a linear dependence on the pump power, and the latter a quadratic dependence. We note that any stray light from the laser and background is excluded by using optical filters and background subtraction. Based on these observations, we can assign the main peak and the new peak at high pump powers to the single-exciton (X) and biexciton (XX) emission, respectively. Their energy separation gives a measure of the biexciton binding energy $\Delta_{XX} = 2E_X^0 - E_{XX}^0$, where E_X^0 and E_{XX}^0 are the exciton and biexciton ground-state energies, respectively [22]. In core-only CdSe QDs, $\Delta_{XX} > 0$ (i.e., the biexciton emission peak appearing toward the red side of the single-exciton peak) has been observed and ascribed to an attractive interaction between excitons [22–24]. The $\Delta_{XX} < 0$ (biexciton emission blueshifted from single-exciton emission) observed in our CdSe/CdS core/shell QDs indicates a repulsive exciton-exciton interaction, which has previously been observed in quasi-type-II and type-II QDs [11,25]. Specifically, the quasi-type-II band structure of the QDs used in this study allows spatial mismatching between the electron and hole wave functions, with the holes being highly confined in the CdSe cores and the electrons delocalized over the whole QD volume [11,26], leading to a local charge quasineutrality [27]. The overall repulsive energy of a biexciton in the QDs used in this study is mainly determined by the repulsion between the two holes confined in the CdSe cores [25]. To determine whether biexciton emission exists in other types of 2D films, we further measure pump-power dependent PL spectra of quasicrystalline 2D films that are 2-monolayer thick [Fig. 1(j)]. Apparent biexciton emission with intensities comparable to that in the 2D films with hexagonal packing can be observed [Figs. 2(c) and 2(f)], indicating that crystalline arrangement of the 2D films likely has a minor influence on the biexciton emission efficiency.

In contrast to the 2D films, the 3D films present much less pronounced biexciton emission at high pump powers, as shown in Fig. 2(b). At the same pump powers, the ratio of

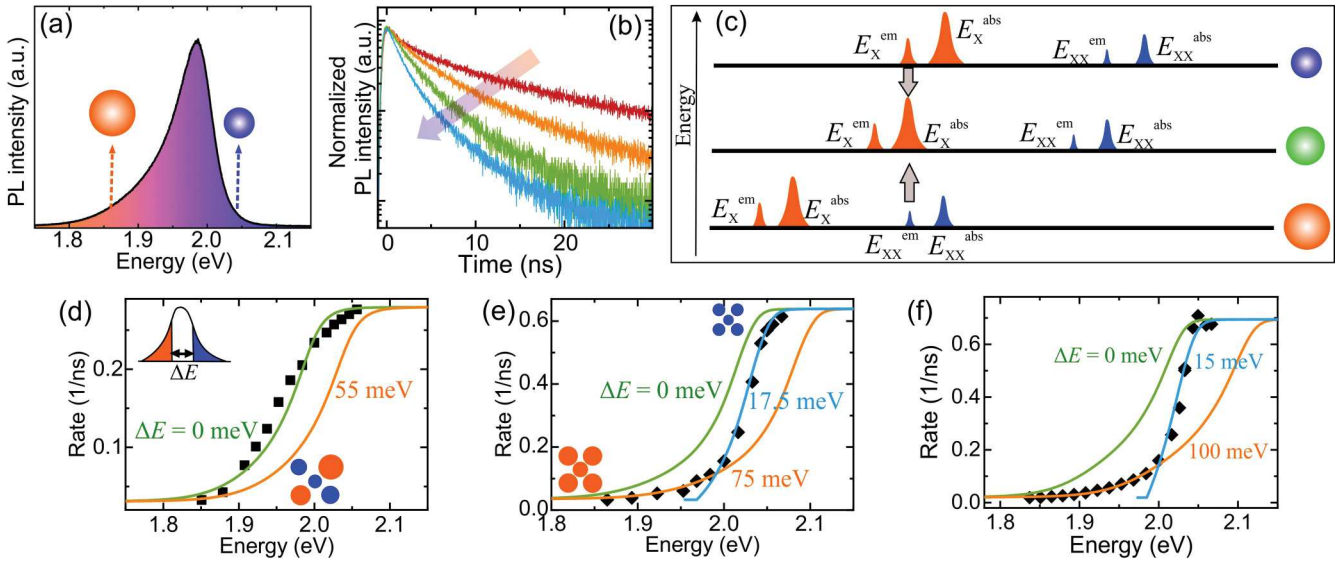

FIG. 3. (a) A PL spectrum of a 3D QD film. (b) Emission energy-dependent PL decay curves of a 3D film. The corresponding emission energies from left to right are 2.06, 2.00, 1.92, and 1.85 eV, respectively. The arrow indicates the trend of the PL decay curves with decreasing QD sizes. (c) Schematic of energy levels contributing to energy transfers in a QD film. (d) Emission energy-dependent decay rates of a 3D film (squares) and the corresponding simulation results (curves). ΔE represents the minimum required energy gap between the donor and acceptor QDs for energy transfer between them to occur. (e) and (f) Emission energy-dependent decay rates of a 2D hexagonal packing (e) and a quasicrystalline (f) film (diamonds) and the corresponding simulation results (curves).

the biexciton and single-exciton emission intensities (I_{XX}/I_X) of the 2D films is significantly larger than that of the 3D films [Figs. 2(g)–2(i)]. This "disappearance" of the biexciton emission in the 3D films can potentially be caused by efficient ET from the biexcitons in donor QDs to adjacent acceptor QDs, as shown in Fig. 3(c). In principle, ET between two QDs is strongly dependent on the donor and acceptor transition dipoles. It is most efficient through resonant coupling between the weak emission transition in the smaller donor QD and the strong absorption transition in the larger acceptor QD [Fig. 3(c), top two rows], which implies the importance of a size difference between the donor-acceptor QDs [7,9]. A similar scenario applies to the biexciton energy transfer, in which the even weaker biexciton emission transition in a donor QD couples to the strong absorption transition in an acceptor QD, except that here the required size difference between the donor and acceptor pair would be reversed due to the negative binding energy of the biexcitons—a larger QD is required as the donor and a smaller QD would serve as the acceptor [Fig. 3(c), bottom two rows]. In this case, instead of undergoing cascade emission, a biexciton in a donor QD would transfer the energy of one of its excitons to a nearby acceptor QD, with the remaining exciton's energy either radiated or transferred to another nearby acceptor QD. Biexciton emission competes with nonradiative Auger recombination processes, both of which typically happen much faster than single-exciton emission. The efficient suppression of biexciton emission in the 3D films indicates that ET could outpace biexciton recombination and it is potentially possible to harvest them for device applications. This observation together with the larger redshift of the 3D films observed in Fig. 2(b) implies that ET is more efficient in the 3D films compared to the 2D films.

B. Spectrally resolved carrier dynamics

This clear difference in the energy transfer efficiencies between the 2D and 3D films may result from two potential mechanisms: variation in the in-plane packing densities and/or difference in the energy transfer rates in the horizontal and vertical directions. For 2D films, the geometrical relaxation in the vertical stacking direction may lead to less ordered structures within the film and this may result in very different energy transfer behavior from that of well-ordered structures. On the other hand, direction-dependent energy transfer rates have previously been observed in Langmuir-Blodgett bilayers [9]. Although the faster horizontal energy transfer rate was attributed to compression-induced smaller interdot separations in the horizontal direction, it remains unknown if such effect exists in naturally packing 3D films.

To understand the mechanism of the different ET efficiencies in the 2D and 3D films, we perform spectrally resolved carrier dynamics studies of the films by recording emission energy-dependent PL decay curves. Figure 3(b) shows representative PL decay curves of a 3D fcc film, with emission at the higher energy side (smaller dots) decaying faster. The PL decay rate decreases with the decreasing emission energy (increasing QD size) and reaches a minimum of $1/33$ ns^{-1} at the lowest energies. This decay rate is identical to that of noninteracting QDs in solutions (Supplemental Material S2 [18]), indicating that for the largest QDs, ET is minimal due to the lack of even larger acceptor QDs. In contrast, the smallest QDs at the highest energy side possess the fastest decay rate of $1/4.0$ ns^{-1} due to their higher probability of undergoing energy transfer. These energy-dependent PL decay dynamics clearly indicate resonant energy transfer from small QDs to large QDs.

To quantify the energy transfer dynamics in the 3D films, we plot the decay rates versus emission energies in Fig. 3(d) (black dots). We then simulate the decay rate $\Gamma(\omega)$ of a QD with an emission energy ω by assuming that $\Gamma(\omega) = \Gamma_0 + \eta(\omega)\Gamma_{ET}$ [7], where Γ_0 and Γ_{ET} are the decay rate of the noninteracting QDs and the energy transfer rate of the QD films, respectively. $\eta(\omega) = \int_0^{\omega-\Delta E} \psi(\omega')d\omega'$ represents the probability of the QD undergoing energy transfer to nearby QDs with band gaps in the range of 0 to $\omega - \Delta E$. ΔE reflects the minimum required energy gap between the donor and acceptor QDs for energy transfer between them to occur; $\psi(\omega')$ here is the normalized size distribution of the QDs reflected in the PL spectra. By assuming all dots with smaller band gaps as viable acceptors (i.e., $\Delta E = 0$), with $\Gamma_0 = 1/33\ \text{ns}^{-1}$, and $\Gamma_{ET} = 1/4.0\ \text{ns}^{-1}$, we find reasonable agreement between the simulation and experimental data [Fig. 3(d), green curve]. This result is considerably different from previous studies of thick QDs drop cast onto substrates [7], in which only QDs with a band gap smaller by $\Delta E = 55$ meV were found to be viable acceptors, which in our case would appear blueshifted from the data [Fig. 3(d), orange curve]. The more efficient energy transfer in our 3D fcc films is likely caused by the closely packed QDs prepared by self-assembly instead of dropcasting.

Compared to the 3D films, the 2D hexagonal packed films show a similar trend with smaller emission energies (larger QDs) corresponding to slower decay rates [Fig. 3(e)]. However, assuming all dots with smaller band gaps as viable acceptors (i.e., $\Delta E = 0$ meV) yields a curve that is apparently redshifted from the 2D film data, in stark contrast to their 3D counterparts. Indeed, the energy dependent decay rates of the 2D films cannot be fit by assuming only a single energy gap; instead, it appears that two major regions exist. The larger QDs with emission energies smaller than 1.98 eV can be well fit by assuming $\Delta E = 75$ meV, whereas the smaller dots with emission energies larger than 1.98 eV have a $\Delta E =$ 17.5 meV. A similar effect can also be observed in the 2D quasicrystalline superlattice films [Fig. 3(f)], indicating that the different energy transfer behavior of the 2D and 3D films is most likely related to the film thickness rather than the crystalline arrangements. The distinct energy transfer regions in the 2D QD films strongly suggest a size-dependent stacking of the QDs, with the larger (emission energy <1.98 eV) and smaller (emission energy >1.98 eV) dots self-assembling into different spatial domains. This size-dependent self-assembly of QDs could be due to the large surface areas of the 2D films. Similar to crystallization of atoms and molecules at a boundary or interface, stacking defects are most easily introduced at the surface [28]. The existence of multiple ordered domains within the 2D films (see the Supplemental Material S3 for TEM images [18]), compared to a more uniform single crystalline superlattice structure in the 3D films, is likely one of the major factors that contribute to the different ET efficiencies in the two types of films.

C. Monte Carlo simulation of the energy transfer processes

We then perform Monte Carlo simulations to examine the influence of domain size on the ET efficiencies of a 2D film. In the simulations, QDs are aligned to form a $N \times N$ 2D hexagonal lattice. Size variation of the dots is represented by introducing a standard deviation to the average band gap value and the resultant energy distribution as a Gaussian function is assigned randomly to each dot. A QD is modeled as a three-level system: an initial laser exited state "3", which relaxes within sub-ns to a band edge state "2". Once there, the QDs can either decay to the ground state "1" at a rate of Γ_0 or energy transfer to a nearby acceptor QD with a rate of Γ_{ET} (see the Supplemental Material S4 for a detailed description [18]). For an exciton sitting on a site i, in a time interval δt, it may hop to one of its 4 (for 2D films) or 12 (for 3D films) nearest neighbor sites j. For simplicity, we focus our discussion here on 2D films with hexagonal arrangements, although it can be extended to a 3D film using the same methodology. In the simulation, a random "decision" number is generated to reflect the exciton's hopping and staying probabilities. The probability for a specific hopping event from site i to j is then [29]

$$P_{i-j} = [1 - \exp(-\delta t)]\frac{\Gamma_{i\to j}}{\sum_{k=1,\ldots,4}\Gamma_{i\to k}}, \tag{1}$$

$$\Gamma_{i\to j} = \Gamma_{ET}\begin{cases} 1, & E_i > E_j, \\ \exp\left(\frac{E_i - E_j}{k_B T}\right), & E_i \leqslant E_j. \end{cases} \tag{2}$$

The sum in Eq. (1) runs over the four nearest neighbor sites $k = 1, \ldots, 4$ of the site i. The term within the bracket in Eq. (1) describes the total hopping probability of an exciton in the time interval δt, and the second term is the chance of it hopping to site j if hopping occurs. In our simulations, we set $\delta t = 0.1$ ns so that it is sufficiently smaller than the decay and energy transfer lifetimes in this study. The term $\exp(\frac{E_i - E_j}{k_B T})$ in Eq. (2) describes uphill hopping weighted by the Boltzmann factor. The duration of the simulation we use is 300 ns to ensure that by the end of each run all the QDs have decayed to the ground state 1. Each time series is then repeated for an iteration number of 20 for good convergence. Data from each run are then averaged.

The ET efficiency is reflected in the average number of hopping steps of the excitons from their initial excitation to their decay into the ground state. Figure 4(a) shows the evolution of exciton populations in 2D hexagonal QD arrays after the initial excitation. The color code in the left three images represents the probability of the QDs in the band edge state 2 (black) and the ground state 1 (light pink) obtained by averaging over 100 iterations. At time $T = 0$ ns, all of the QDs are in the band edge state 2. As time proceeds, more and more QDs decay into the ground state 1 after certain steps of energy transfer. As can be seen in Figs. 4(b) and 4(c), the excitons' average hopping steps in 2D hexagonal QD films increase with the domain size N initially and then saturate to a maximum value of around 15 for domain size $N \sim 100$, in a reasonable agreement with previously reported values [30]. This suggests that in large enough domains, exciton decay rather than domain boundary becomes the limiting factor. Our TEM analysis of the 2D films with hexagonal arrangement gives an average domain size of $N \sim 60$ (Supplemental Material S3 [18]), smaller than the saturation value. This further confirms our conclusion from the carrier dynamics studies in Figs. 3(e) and 3(f) that the existence of domain boundaries in 2D films contributes to the reduced energy

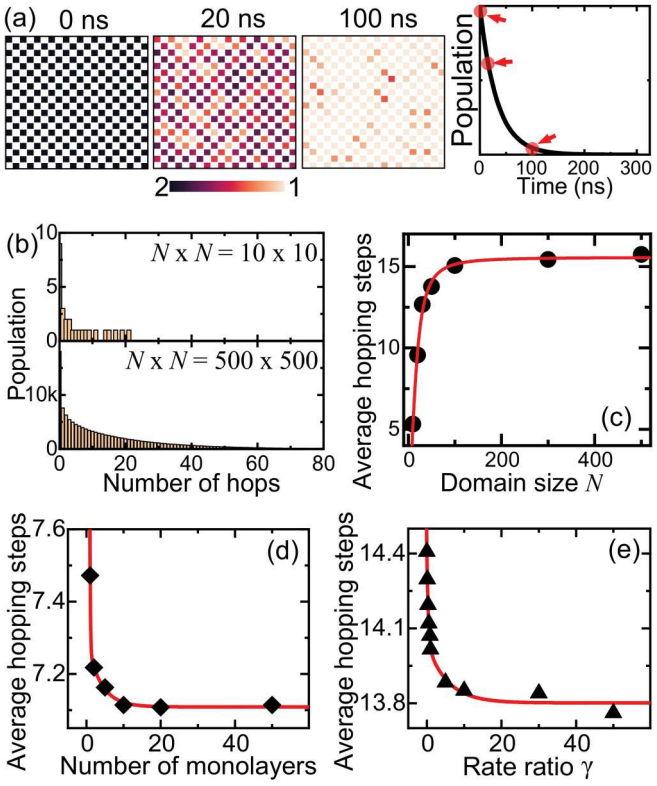

FIG. 4. (a) Monte Carlo simulations of exciton population evolution after the initial optical excitation. The left three images show the distributions of QDs in a 20×20 2D hexagonal QD array between the band edge state 2 (black) and the ground state 1 (light pink) at various times (0, 20, and 100 ns) after the initial excitation. The color code represents the probability of the QDs at the two states obtained by averaging over 100 iterations. A deeper color indicates that the QD is more likely to be at the band edge state 2 and a lighter color to be at the ground state 1. The right plot shows the time-dependent population evolution of excitons remaining at the band edge state 2 in a 100×100 2D hexagonal lattice. The exciton populations corresponding to the times in the left three images are highlighted. (b) Histograms of hopping steps of a 10×10 and a 500×500 2D hexagonal lattices. (c) Domain size N-dependent average exciton hopping steps in the 2D hexagonal lattices. The exciton decay rate $\Gamma_0 = 1/33$ ns^{-1} and the energy transfer rate $\Gamma_{ET} = 1/1.6$ ns^{-1}. (d) QD film thickness-dependent exciton hopping steps. Here the size of the QD film is $100\times100\times M$, with M being the number of monolayers in the vertical direction. The exciton decay rate $\Gamma_0 = 1/33$ ns^{-1} and the energy transfer rate $\Gamma_{ET} = 1/4.0$ ns^{-1}. (e) Rate ratio γ-dependent average exciton hopping steps. γ is defined as the ratio between the vertical and in-plane energy transfer rates.

transfer efficiencies. We also note that despite the less efficient ET in the 2D films caused by the defect-induced domains, their absolute ET rate ($1/1.6$ ns^{-1}) could actually be larger than that of the 3D films ($1/4.0$ ns^{-1}), consistent with previous studies [9,10]. This seemingly contradicting finding can be attributed to the multiple domains in the 2D films: while each domain could have fast ET rates, the domain boundary limits the overall ET efficiencies. This finding suggests that aside from ET rates, formation of uniform films is also essential to ensure long distance ET throughout the film.

We also examine the influence of "vertical" interlayer ET rates using Monte Carlo simulations. By assuming the same in-plane ($\Gamma_{ET,\parallel}$) and vertical ($\Gamma_{ET,\perp}$) ET rates in a $100\times100\times M$ 3D fcc array, where M is the number of monolayers in the vertical direction, we find that the film thickness has a minimal influence on the exciton hopping steps, although a very small decrease in the hopping steps can be observed for the first 20 monolayers [Fig. 4(d)]. Note that the exciton decay and transfer rates used here are those of the 3D films, hence the smaller hopping steps compared to that in Fig. 4(c). Finally, we keep the 3D film thickness to 20 monolayers of QDs, the in-plane ET rate to $\Gamma_{ET,\parallel} = 1/1.6$ ns^{-1}, and tune the vertical ET rate by altering the rate ratio $\gamma = \Gamma_{ET,\perp}/\Gamma_{ET,\parallel}$. The exciton hopping steps first decrease with an increasing vertical ET rate $\Gamma_{ET,\perp}$ until it reaches a constant value [Fig. 4(e)]. However, consistent with the data in Fig. 4(d), the ET rate in the vertical direction has a small effect on the overall exciton hopping steps. These observations show that the difference in the energy transfer efficiencies between the 2D and 3D films is mainly caused by the packing densities and film homogeneity, while difference in the in-plane and interlayer ET rates has a much smaller effect. Overall, ET efficiencies of QD films are not only related to the ET rates, but also the microscopic local film structures. While ET rate sets a macroscopic upper limit, the local film geometry and the specific ET channels have a noteworthy influence on the overall ET efficiencies as well.

IV. CONCLUSIONS

In summary, we study the influence of local structures on the energy transfer processes in 2D and 3D QD films. Using pump power-dependent PL spectroscopy, we find that biexciton emission in the 3D films is effectively suppressed, likely due to efficient energy transfer processes. Combining carrier dynamics measurements with Monte Carlo simulations, we find that very much similar to crystallization of atoms and molecules at a boundary or interface, in which stacking defects are most easily introduced at the surface, thin 2D films tend to form spatial domains of QDs. This existence of multiple ordered domains in the 2D films causes perturbations to local QD arrangements. While each domain could have very fast energy transfer rates, thus giving rise to a faster energy transfer rate, the domain boundary limits the overall exciton hopping distances and ET efficiencies. This scenario is reversed in the 3D QD films, which tend to form uniform crystalline arrangements that allow higher ET efficiencies. Moreover, our simulations indicate a much less pronounced effect from anisotropic ET rates in the in-plane and vertical directions. Our study highlights the importance of film homogeneity on the ET efficiencies and suggests that in devices with predominant microscopic structures, it is critical to consider the effect of local structures on the overall energy transfer processes. These findings have practical implications for the design of efficient optoelectronic [31] and light harvesting devices [32,33] based on quantum emitters with discrete energy levels.

ACKNOWLEDGMENTS

We acknowledge support from the National Science Foundation DMR Program under the Award No. DMR-1905990. O.C. acknowledges support from Brown University startup fund and partial financial support from National Science Foundation (DMR-1943930 and CMMI-1934314). TEM measurements were performed at the Electron Microscopy Facility in the Institute for Molecular and Nanoscale Innovation (IMNI) at the Brown University. Use of the Center for Nanoscale Materials, an Office of Science user facility, was supported by the U.S. Department of Energy, Office of Science, Office of Basic Energy Sciences, under Contract No. DE-AC02-06CH11357.

[1] T. Forster, Naturwissenschaften **33**, 166 (1946).

[2] D. Shrestha, A. Jenei, P. Nagy, G. Vereb, and J. Szöllősi, Int. J. Mol. Sci. **16**, 6718 (2015).

[3] C. Tummeltshammer, M. Portnoi, S. A. Mitchell, A.-T. Lee, A. J. Kenyon, A. B. Tabor, and I. Papakonstantinou, Nano Energy **32**, 263 (2017).

[4] K. Wu, H. Li, and V. I. Klimov, Nat. Photon. **12**, 105 (2018).

[5] J. B. Sambur, T. Novet, and B. A. Parkinson, Science **330**, 63 (2010).

[6] B. Farrow and P. V. Kamat, J. Am. Chem. Soc. **131**, 11124 (2009).

[7] S. A. Crooker, J. A. Hollingsworth, S. Tretiak, and V. I. Klimov, Phys. Rev. Lett. **89**, 186802 (2002).

[8] K. Zheng, K. Žídek, M. Abdellah, N. Zhu, P. Chábera, N. Lenngren, Q. Chi, and T. Pullerits, J. Am. Chem. Soc. **136**, 6259 (2014).

[9] M. Achermann, M. A. Petruska, S. A. Crooker, and V. I. Klimov, J. Phys. Chem. B **107**, 13782 (2003).

[10] M. Achermann, S. Jeong, L. Balet, G. A. Montano, and J. A. Hollingsworth, ACS Nano **5**, 1761 (2011).

[11] H. Htoon, A. V. Malko, D. Bussian, J. Vela, Y. Chen, J. A. Hoolingsworth, and V. I. Klimov, Nano Lett. **10**, 2401 (2010).

[12] Y. Louyer, L. Biadala, J.-B. Trebbia, M. J. Fernee, P. Tamarat, and B. Lounis, Nano Lett. **11**, 4370 (2011).

[13] J. Q. Grim, S. Christodoulou, F. D. Stasio, R. Krahne, R. Cingolani, L. Manna, and I. Moreels, Nat. Nanotechnol. **9**, 891 (2014).

[14] X. Ma, B. T. Diroll, W. Cho, I. Fedin, R. D. Schaller, D. V. Talapin, S. K. Gray, G. P. Wiederrecht, and D. J. Gosztola, ACS Nano **11**, 9119 (2017).

[15] L. Peng, M. Otten, A. Hazarika, I. Coropceanu, M. Cygorek, G. P. Wiederrecht, P. Hawrylak, D. V. Talapin, and X. Ma, Phys. Rev. Materials **4**, 056006 (2020).

[16] G. Soavi, S. D. Conte, C. Manzoni, D. Viola, A. Narita, Y. Hu, X. Feng, U. Hohenester, E. Molinari, D. Prezz, K. Müller, and G. Cerullo, Nat. Commun. **7**, 11010 (2016).

[17] R. Tan, Y. Yuan, Y. Nagaoka, D. Eggert, X. Wang, S. Thota, P. Guo, H. Yang, J. Zhao, and O. Chen, Chem. Mater. **29**, 4097 (2017).

[18] See Supplemental Material at http://link.aps.org/supplemental/10.1103/PhysRevB.102.035437 for details of experiments and simulations.

[19] Y. Nagaoka, R. Tan, R. Li, H. Zhu, D. Eggert, Y. A. Wu, Y. Liu, Z. Wang, and O. Chen, Nature **561**, 378 (2018).

[20] Y. Nagaoka, H. Zhu, D. Eggert, and O. Chen, Science **362**, 1396 (2018).

[21] J. van Embden, J. E. Sader, M. Davidson, and P. Mulvaney, J. Phys. Chem. C **113**, 16342 (2009).

[22] S. L. Sewall, A. Franceschetti, R. R. Cooney, A. Zunger, and P. Kambhampati, Phys. Rev. B **80**, 081310(R) (2009).

[23] M. Achermann, J. A. Hollingsworth, and V. I. Klimov, Phys. Rev. B **68**, 245302 (2003).

[24] J.-M. Caruge, Y. Chan, V. Sundar, H. J. Eisler, and M. G. Bawendi, Phys. Rev. B **70**, 085316 (2004).

[25] Z. Deutsch, A. Avidan, I. Pinkas, and D. Oron, Phys. Chem. Chem. Phys. **13**, 3210 (2011).

[26] A. Sitt, F. D. Sala, G. Menagen, and U. Banin, Nano Lett. **9**, 3470 (2009).

[27] A. L. Efros and A. V. Rodina, Solid State Commun. **7**, 645 (1989).

[28] J. Gong, R. S. Newman, M. Engel, M. Zhao, F. Bian, S. C. Glotzer, and Z. Tang, Nat. Commun. **8**, 14038 (2017).

[29] Y. Gao, C. S. S. Sandeep, J. M. Schins, A. J. Houtepen, and L. D. A. Siebbeles, Nat. Commun. **4**, 2329 (2013).

[30] N. Kholmicheva, P. Moroz, E. Bastola, N. Razgoniaeva, J. Bocanegra, M. Shaughnessy, Z. Porach, D. Khon, and M. Zamkov, ACS Nano **9**, 2926 (2015).

[31] J. Wu, S. Chen, A. Seeds, and H. Liu, J. Phys. D: Appl. Phys. **48**, 363001 (2015).

[32] I. Nabiev, A. Rakovich, A. Sukhanova, E. Lukashev, V. Zagidullin, V. Pashenko, Y. P. Rakovich, J. F. Donegan, A. B. Rubin, and A. O. Govorov, Angew. Chem. Int. Ed. **49**, 7217 (2010).

[33] P. V. Kamat, J. Phys. Chem. C **112**, 18737 (2008).